Conference on Modelling Fluid Flow (CMFF'09)
The 14th International Conference on Fluid Flow Technologies
Budapest, Hungary, September 9-12, 2009

Numerical Method to Predict Interactions between Free-Surface Flows and Elastic Bodies

Satoru Ushijima[1] and Nozomu Kuroda[2]

[1] Kyoto University, ACCMS, Kyoto-shi, 606-8501, Japan, E-mail:ushijima@mbox.kudpc.kyoto-u.ac.jp
[2] Kyoto University, CERE, Kyoto-shi, 615-8540, Japan

ABSTRACT

This paper deals with a computational method to predict the interactions between three-dimensional free-surface flows and elastic bodies. The free-surface flow including solid objects is modeled as a multiphase flow field. The governing equations for the field are solved on the basis of a finite-volume method with collocated grid system. A solid object, which is treated as a linear elastic body, is represented with multiple tetrahedron elements and their deformations are solved with a finite-element method (FEM). The fluid forces acting on the solid bodies are evaluated from the volume integral of the calculated momentum equations corresponding to the solid area. Since the fluid-solid interactions are taken into account, no additional constants, such as the drag and lift coefficients, are needed in the present method. As a result of the comparisons with experiments, it was shown that the present computational method enables us to predict the interactions between wave-induced free-surface flows and the deformations of elastic bodies in the flows.

Keywords : fluid-solid interaction, free-surface flow, elastic body, fluid force, multiphase model

NOMENCLATURE

C	$[N \cdot sec/m]$	dumping matrix
L	$[1/sec]$	velocity gradient tensor
M	$[kg]$	mass matrix
T	$[Pa]$	Cauchy stress tensor
$\boldsymbol{d}$	$[m]$	displacement vector
p	$[Pa]$	volume-averaged pressure
t	$[s]$	time
u_i	$[m/s]$	mass-averaged velocity
x_i	$[m]$	orthogonal coordinates
μ	$[m^2/s]$	viscous coefficient
ρ	$[kg/m^3]$	volume-averaged density

1. INTRODUCTION

The accurate evaluation of the interactions between free-surface flows and deformable objects is an important engineering subject. In the present study, a flexible object is represented by multiple tetrahedron elements and its finite deformation is calculated with FEM. This solid model is implemented in a multiphase-flow model in order to deal with the fluid-solid interaction. In the multiphase-flow model, the free-surface flow including solid objects, which consists of gas, liquid and solid phases, is modeled as a mixture of the immiscible and incompressible different fluids. The fluid forces acting on the objects are calculated from the computational results of the momentum equation in the multiphase-flow model. The predicted displacement velocities of the objects are then used to determine the mass-averaged velocities in the multiphase field.

The computational method was applied to the experiments to confirm its applicability. As a result, it was shown that the deformations of elastic plates and the fluid forces due to the wave-induced flows are reasonably predicted with the present method.

2. NUMERICALPROCEDURES

2.1. Basic Equations

The multiphase field Ω consisting of gas, liquid and solid phases is treated as a mixture of fluids, which is the collection of the immiscible and incompressible fluids Ω_i, as shown in Figure 1. The fluid components Ω_i in Fig.1 have different densities and viscous coefficients equivalent to the corresponding phases.

Assuming that the volume of Ω is sufficiently

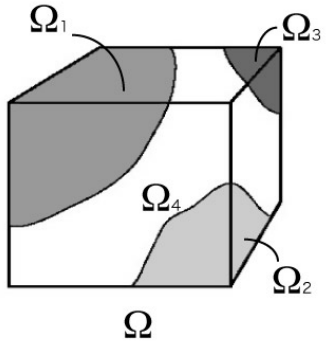

Figure 1. Mixture of immiscible and incompressible fluids

small, a variable $\phi_k^{'}(t, \boldsymbol{x})$ in each fluid is approximated as its spatially-representative value $\phi_k(t)$ as follows:

$$\int_{\Omega_k} \phi_k^{'}(t, \boldsymbol{x})\ d\Omega \approx \Omega_k \phi_k(t) \tag{1}$$

where Ω_k is the volume of the fluid-k. With Eq.(1), the mass-conservation equation for Ω in the Eulerian form can be written as

$$\frac{\partial \rho}{\partial t} + \frac{\partial}{\partial x_j}(\rho u_j) = 0 \tag{2}$$

where ρ and u_i are volume-average density and mass-average velocity component:

$$\rho = \frac{\sum_k \Omega_k \rho_k}{\Omega}, \qquad u_i = \frac{\sum_k \Omega_k \rho_k u_{k,i}}{\Omega \rho} \tag{3}$$

Similarly, with the assumption that the difference between u_i and $u_{k,i}$, which is the velocity component of the fluid-k, is negligible, the mass-conservation equation in the Lagrangian form is given by

$$\frac{\partial \rho}{\partial t} + u_j \frac{\partial \rho}{\partial x_j} = 0 \tag{4}$$

From Eqs.(2) and (4), the following incompressible condition is derived:

$$\frac{\partial u_j}{\partial x_j} = 0 \tag{5}$$

With the similar procedures, the momentum equation is derived as follows:

$$\begin{aligned} &\frac{\partial u_i}{\partial t} + \frac{\partial}{\partial x_j}(u_i u_j) = f_i \\ &- \frac{1}{\rho}\frac{\partial p}{\partial x_i} + \frac{1}{\rho}\frac{\partial}{\partial x_j}\left[\frac{\partial}{\partial x_j}(\mu u_i) + \frac{\partial}{\partial x_i}(\mu u_j)\right] \end{aligned} \tag{6}$$

where f_i is the acceleration component of the body force, while p and μ are volume-average pressure and viscous coefficient defined as

$$p = \frac{\sum_k \Omega_k p_k}{\Omega}, \qquad \mu = \frac{\sum_k \Omega_k \mu_k}{\Omega} \tag{7}$$

2.2. Computational Method

The discretised governing equations of the fluid-mixture are solved after determining the volume-average physical properties with the subcell method, which will be described later. The velocity components u_i and the pressure variable p of the discretised governing equations are defined on the collocated grid points in the computational fluid-cell.

The numerical procedures of the incompressible fluid-mixture consist of three stages; prediction, pressure-computation and correction stages. At the prediction stage, the tentative velocity components u_i^* are calculated at the center of the fluid-cells with a finite-volume method. In this procedure, Eq.(6) is discretised with the C-ISMAC method [1], which is based on the implicit SMAC method [2]. The equation discretised with respect to time by the C-ISMAC method is given by

$$\begin{aligned} &\frac{u_i^* - u_i^n}{\Delta t} = f_i - \frac{1}{\rho}\frac{\partial p^n}{\partial x_i} \\ &- \alpha \frac{\partial}{\partial x_j}(u_i^* u_j^n) - (1-\alpha)\frac{\partial}{\partial x_j}(u_i^n u_j^n) \\ &+ \frac{\beta}{\rho}\frac{\partial}{\partial x_j}\left[\frac{\partial}{\partial x_j}(\mu u_i^*) + \frac{\partial}{\partial x_i}(\mu u_j^*)\right] \\ &+ \frac{1-\beta}{\rho}\frac{\partial}{\partial x_j}\left[\frac{\partial}{\partial x_j}(\mu u_i^n) + \frac{\partial}{\partial x_i}(\mu u_j^n)\right] \end{aligned} \tag{8}$$

where α and β are parameters whose ranges are $0 \le \alpha, \beta \le 1$. With the following relationship,

$$u_i^* = u_i^n + \tilde{u}_i \tag{9}$$

Eq.(8) is transformed to the following equation:

$$\begin{aligned} &\frac{\tilde{u}_i}{\Delta t} + \alpha \frac{\partial}{\partial x_j}(\tilde{u}_i u_j^n) - \frac{\beta}{\rho}\frac{\partial}{\partial x_j}\left[\frac{\partial}{\partial x_j}(\mu \tilde{u}_i) + \frac{\partial}{\partial x_i}(\mu \tilde{u}_j)\right] \\ &= f_i - \frac{1}{\rho}\frac{\partial p^n}{\partial x_i} - \frac{\partial}{\partial x_j}(u_i^n u_j^n) \\ &+ \frac{1}{\rho}\frac{\partial}{\partial x_j}\left[\frac{\partial}{\partial x_j}(\mu u_i^n) + \frac{\partial}{\partial x_i}(\mu u_j^n)\right] \end{aligned} \tag{10}$$

where $\tilde{u}_i$ becomes nearly zero when the flow field is almost steady or the time-scale of the flow field is sufficiently larger than the time increment Δt. Thus, we can apply a simple first-order spatial discretisation method to the left-hand side of Eq.(10), while a higher-order scheme to the right-hand side. The convection terms are evaluated with a fifth-order conservation FVM-QSI scheme [3] and numerical oscillations are removed by a flux-control method [3]. The C-ISMAC method enables us to derive easily the simultaneous equation system from the implicit form of the left-hand side of Eq.(10) as well as

to preserve numerical accuracy by applying a higher-order scheme to the explicit form on the right-hand side of the same equation.

After solving the equation system of $\tilde{u}_i$, which is derived from the discretised equation of Eq.(10), u_i^* is determined with Eq.(9). The u_i^* located at the center of the fluid-cell is then spatially interpolated on the cell boundary. Before this interpolation, pressure-gradient term evaluated at the cell center is removed from u_i^* in order to prevent pressure oscillation as

$$\hat{u}_i = u_i^* + \frac{1}{\rho}\frac{\partial p^n}{\partial x_i}\Delta t \tag{11}$$

The cell-center velocity $\hat{u}_i$, which is evaluated without the pressure-gradient term, is spatially interpolated on the cell boundaries by a suitable function f_b. After this procedure, the pressure-gradient terms that are estimated on the cell boundaries are added to the interpolated velocity, $f_b(\hat{u}_i)$. Thus, we obtain the cell-boundary velocity component $u_{b,i}$ as follows:

$$u_{b,i} = f_b(\hat{u}_i) - \frac{1}{\rho}\frac{\partial p^n}{\partial x_i}\bigg|_b \Delta t \tag{12}$$

The velocity component $u_{b,i}^{n+1}$ at $n+1$ time-step is defined by

$$u_{b,i}^{n+1} = f_b(\hat{u}_i) - \frac{1}{\rho}\frac{\partial p^{n+1}}{\partial x_i}\bigg|_b \Delta t \tag{13}$$

Subtracting Eq.(12) from Eq.(13), we have

$$u_{b,i}^{n+1} = u_{b,i} - \frac{1}{\rho}\frac{\partial \phi}{\partial x_i}\Delta t \tag{14}$$

where $\phi = p^{n+1} - p^n$. Substitution of Eq.(14) into Eq.(5) yields the following equation of ϕ :

$$\frac{\partial}{\partial x_i}\left(\frac{1}{\rho}\frac{\partial \phi^k}{\partial x_i}\right) = \frac{1}{\Delta t}\frac{\partial u_{b,i}}{\partial x_i} \equiv \frac{D}{\Delta t} \tag{15}$$

At the pressure-computation stage, Eq.(15) is solved with the C-HSMAC method. The C-HSMAC method enables us to obtain the pressure and cell-boundary velocity components, which satisfy the incompressible condition $|D| < \epsilon_D$ in each computational cell, where ϵ_D is a given threshold. While the final results of the C-HSMAC method are similar to those of the SOLA method [4], it has been proved that the computational efficiency of the C-HSMAC method is largely improved [5]. The relationships in the C-HSMAC method are given by

$$\frac{\partial}{\partial x_i}\left(\frac{1}{\rho}\frac{\partial \phi}{\partial x_i}\right) = \frac{D^k}{\Delta t} \tag{16}$$

$$p^{k+1} = p^k + \phi \tag{17}$$

$$u_{b,i}^{k+1} = u_{b,i}^k - \frac{\Delta t}{\rho}\frac{\partial \phi}{\partial x_i} \tag{18}$$

where the superscript k stands for the iteration step-number of the C-HSMAC method.

The discretisation of Eq.(16) yields simultaneous linear equation system of ϕ, which is solved with the BiCGSTAB method [6]. The iterative computation using the above three equations is completed when $|D| < \epsilon_D$ is satisfied in all fluid-cells.

2.3. Solid Model

The solid object is represented with the multiple tetrahedron elements. Each element has ten computational nodes used in FEM. The shape function N_i $(i = 1, \cdots, 10)$ in an element is given by a quadratic function of the natural coordinates in the corresponding isoparametric element. When the displacement vector $\boldsymbol{d}$ on the node is approximated with N_i, the following relationship can be derived:

$$M\ddot{\boldsymbol{d}} + C\dot{\boldsymbol{d}} + \boldsymbol{F}_{int} = \boldsymbol{f} \tag{19}$$

where $\boldsymbol{f}$ and $\boldsymbol{F}_{int}$ are the external and internal force vectors acting on the node, while M and C are mass and damping matrices, which are given by diagonal forms.

A solid object treated in this study is assumed to be a linear elastic body. Thus, the stress-strain behavior of the material is given by a linear constitutive relation, while the finite deformation, which is related to the geometric nonlinearity [7], is taken into account. In order to deal with the large deformation, the following objective stress rate, Cotter-Rivlin stress rate tensor $\dot{T}_c$, is utilized [8]:

$$\dot{T}_c = \dot{T} + L^T T + TL \tag{20}$$

where T and L are Cauchy stress and velocity gradient tensors, respectively. The $\dot{T}_c$ is evaluated with the following time derivative of the linear constitutive relation:

$$\{\dot{T}_c\}_v = D\dot{\boldsymbol{\epsilon}} = DB\dot{\boldsymbol{d}} \tag{21}$$

where $\{\ \}_v$ means the vector form of the tensor, while $\boldsymbol{\epsilon}$, D and B are the strain vector on nodes, stress-strain and strain-displacement matrices respectively. The stress tensor at $n+1$ time step given by T^{n+1} is approximated with the Euler explicit discretisation:

$$\{T^{n+1}\}_v = \{T^n\}_v + \{\dot{T}\}_v \Delta t \tag{22}$$

where $\dot{T}$ is obtained from Eq.(20). Then, $\boldsymbol{F}_{int}^{n+1}$ in Eq.(19) is calculated with the following volume integral:

$$\boldsymbol{F}_{int}^{n+1} = \int_{\Omega} \boldsymbol{B}^T \{T^{n+1}\}_v d\Omega \tag{23}$$

Finally, the acceleration vector $\ddot{\boldsymbol{d}}$ is calculated from Eq.(19) with the following equation:

$$\ddot{\boldsymbol{d}} = M^{-1}\left[\boldsymbol{f} - C\dot{\boldsymbol{d}} - \boldsymbol{F}_{int}\right] \tag{24}$$

The node velocity vector $\dot{\boldsymbol{d}}$ and displacement vector $\boldsymbol{d}$ can be obtained by the numerical time integration of Eq.(24).

2.4. Interactions between Fluids and Objects

As shown in the governing equations, the physical values of the mixture of fluids need to be determined for each fluid cell. Since the fluid cell is based on the Eulerian grid fixed in the space, the volume-average physical value ψ in the cell C is estimated with the following equation:

$$\psi = (1-f)\psi_g + \left(f - \sum_{O_k \in C} \alpha_k\right)\psi_l + \sum_{O_k \in C} \alpha_k \psi_{bk} \tag{25}$$

where ψ_g, ψ_l and ψ_{bk} are physical values in gas, liquid phases and the object-k, O_k in Eq.(25), respectively. The volume fraction of liquid and solid phases in a fluid-cell is given by f in Eq.(25), while the fraction of the solid part is defined by α_k. The fraction α_k is approximated with a sub-cell method, as illustrated in Figure 2. When an element is included in the multiple fluid-cells as shown in Fig.2, each fluid-cell is divided into multiple sub-cells and α_k is determined from the number of sub-cells included in the element.

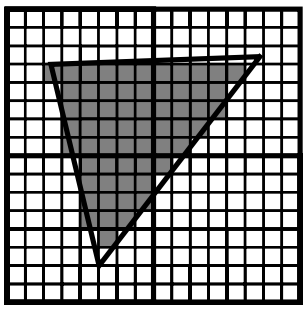

Figure 2. Sub-cell method (thick and thin grid lines stand for fluid-cell and sub-cell boundaries)

The fluid forces acting on the objects are calculated with the pressure and viscous terms in the computational results of Eq.(6). The fluid force vector $\boldsymbol{F}_{Ckm}$ acting on a part of the element T_{km} of the object-k included in a fluid-cell C is evaluated as the following procedures. The x_i component of $\boldsymbol{F}_{Ckm}$, which is given by F_{Ckm}^i, is calculated with a portion of the element volume ΔT_{Ckm} included in the fluid-cell C and the density ρ_{bk} of the object-k as

$$F_{Ckm}^i = \rho_{bk}\Delta T_{Ckm}\left[-\frac{1}{\rho}\frac{\partial p}{\partial x_i} + \frac{1}{\rho}\frac{\partial}{\partial x_j}\left\{\frac{\partial}{\partial x_j}(\mu u_i) + \frac{\partial}{\partial x_i}(\mu u_j)\right\}\right] \tag{26}$$

where ΔT_{Ckm} is evaluated with the sub-cell method.

To calculate the deformation of the solid objects, the fluid force calculated with Eq.(26) is distributed to ten nodes in an element and it is used as the external force $\boldsymbol{f}$ in Eq.(24). On the other hand, the calculated displacement velocity vector $\dot{\boldsymbol{d}}$ on the node is taken into account in the multiphase field. The velocity vector $\boldsymbol{v}_{km}$ of the element T_{km} is determined as the average value of those defined at the nodes $\dot{\boldsymbol{d}}$. The contribution of the element T_{km} to the fluid-cell C is then determined with $\boldsymbol{v}_{km}$, density and volume ΔT_{Ckm}. Finally, the velocity vector $\boldsymbol{u}$ in the multiphase field, is determined as the following mass-averaged value:

$$\boldsymbol{u} = \frac{1}{m_C}\left(m_f \boldsymbol{u}_f + \sum_k \sum_m \rho_{bk}\Delta T_{Ckm}\boldsymbol{v}_{km}\right) \tag{27}$$

where m_C and m_f are total mass in the fluid-cell and the mass of gas and liquid phases, respectively. The velocity vector of the mixture of gas and liquid phases is given by $\boldsymbol{u}_f$.

3. APPLICABILITY OF PREDICTION METHOD

The computational method was applied to the experimental results to confirm its applicability. As shown in Figure 3, the deformation of an elastic plate was measured in a water tank equipped with a wave generator. The deformation of the plate is caused by the wave-induced flow generated on a box in the water tank shown in Fig.3. The top of the elastic plate is fixed on a steel plate, on which four strain gages are attached to measure the fluid forces acting on the elastic plate. The lengths of the tank L_1, L_2 and B shown in Fig.3 are 0.7 m, 0.7 m and 0.19 m, while the initial water depth h_0 and the

height of the box h_b are 0.15 m and 0.1 m, respectively. The bottom surface of the elastic plate is placed 15mm above the top of the box. The specific gravity, the Young's modulus and dumping coefficient per unit volume of the elastic plate are about 0.255, 3.5×10^5 Pa and 2.0×10^3 N s/m/m^3, respectively.

In the experiments, the maximum water depth h_m in front of the box was 195 mm. The deformations of the elastic plate were recorded by a video camera and the displacements were evaluated with the image analysis. In addition, the fluid forces were measured by the strain gages on the supporting steel plate.

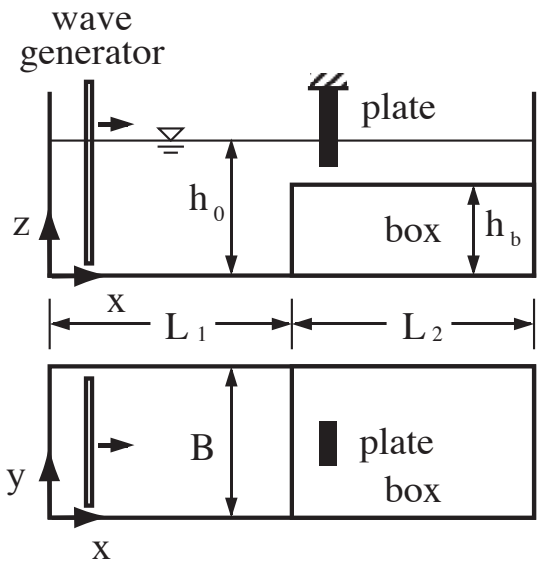

Figure 3. Water tank used in experiments (side and plane views)

In the computations, a fluid-cell is a $10 \times 10 \times 10$ mm cube and $140 \times 19 \times 25$ cells were set for the regions inside of the tank, including water, air and the elastic plate. The kinematic viscosities of water and air are set at 1.0×10^{-6} and 1.0×10^{-5} m^2/s, while their densities are 1.0×10^3 and 1.0 kg/m^3 respectively. The elastic plate is represented by 164 tetrahedron elements with 441 nodes.

Figure 4 shows the time histories of the displacements dt at the bottom of the elastic plate. Since the predicted results generally agree with the experimentally-observed displacements in both cases, it can be thought that the present solid model for finite deformation is effective.

The comparison between experiments and predictions regarding the fluid forces F_w acting on the plate is shown in Figure 5. While the calculated fluid forces are slightly smaller than those obtained in experiments, the shapes of the distributions are reasonably predicted.

The pressure distributions around the deformed plate are shown in Figure 6. It can be seen that the high pressure regions exist on the upstream ($-x$ direction) side of the wave-induced flow, while on the downstream side low pressure zone arises due to the wake vortex flows. It can be concluded that the adequate evaluation of the surrounding pressure field enables us to obtain the reasonably-predicted results as shown in Figs.4 and 5.

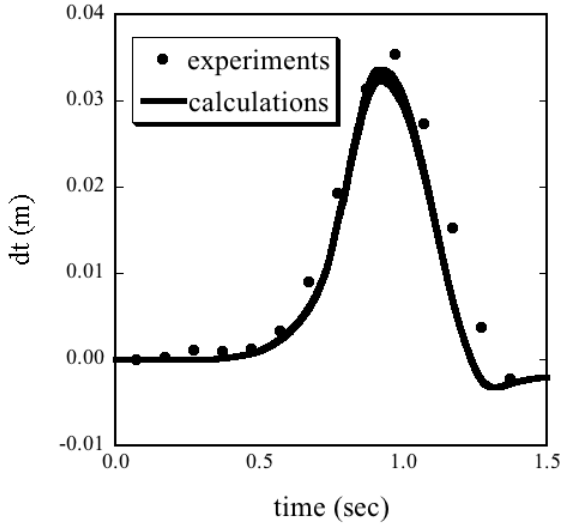

Figure 4. Time history of displacement

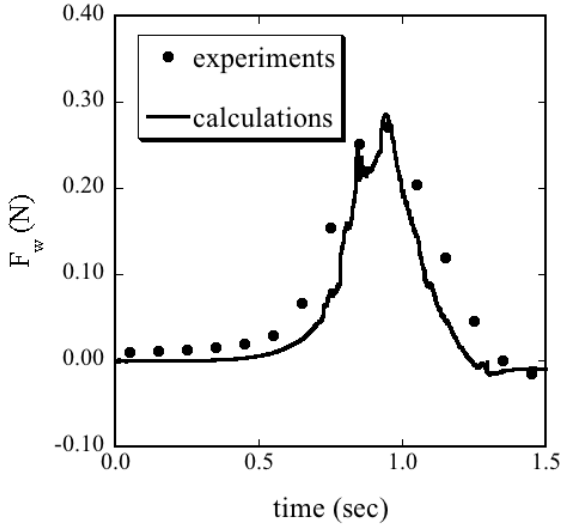

Figure 5. Time history of fluid force

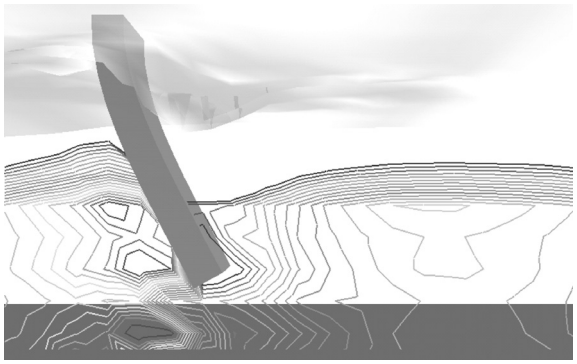

(a) side view

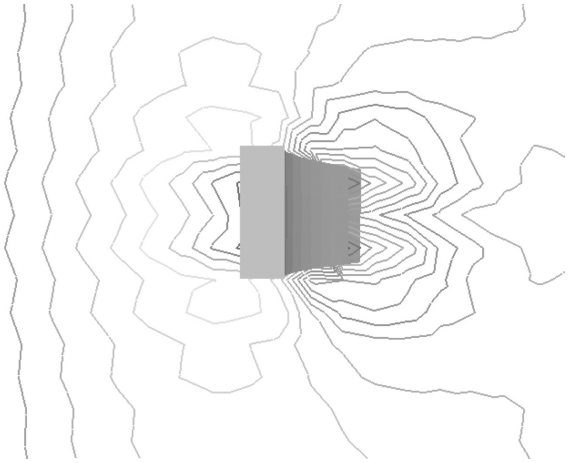

(b) top view

Figure 6. Predicted pressure distributions around deformed plate

CONCLUSIONS

A computational method was proposed on the basis of the multiphase modeling to predict the interactions between free-surface flows and the linear elastic objects which undergo finite deformations. In the multiphase modeling, the gas, liquid and solid phases are treated as immiscible and incompressible fluids and the governing equations are derived. The solid model, on the other hand, is derived with the objective stress rates to deal with the finite deformations. The proposed computational method was applied to the experimental results: deformations of an elastic plate due to wave-induced flows. As a result, it was shown that the plate displacements and fluid forces are successfully predicted with the present method.

REFERENCES

[1] Ushijima, S. and Nezu, I., 2002, "Higher-order implicit (C-ISMAC) method for incompressible flows with collocated grid system", *JSCE Journal*, No. 719/II-61, pp. 21–30.

[2] Shin, B. R., Ikohagi, T. and Daiguji, H., 1993, "An unsteady implicit SMAC scheme for two-dimensional incompressible Navier-Stokes equations", *JSME International Journal*, Vol. 36, No. 4, pp. 598–606.

[3] Ushijima, S., Yoshida, K., Takemura, M. and Nezu, I., 2003, "Fifth-order conservative scheme with flux control applicable to convection equations", *JSCE Journal*, No. 747/II-65, pp. 85–94.

[4] Hirt, C. W. and Cook, J. L., 1972, "Calculating three-dimensional flows around structures and over rough terrain", *J. Comput. Phys.*, Vol. 10, pp. 324–340.

[5] Ushijima, S., Yamada, S., Fujioka, S. and Nezu, I., 2006, "Prediction method (3D MICS) for transportation of solid bodies in 3D free-surface flows", *JSCE Journal*, Vol. 810/II-74, pp. 79–89.

[6] Vorst, H. A. V. D.: BI-CGSTAB, 1992, "A first and smoothly converging variant of BI-CG for the solution of nonsymmetric linear systems", *SIAM J. Sci. Stat. Comput.*, Vol. 13, pp. 631–644.

[7] Bonet, J. and Wood, R. D., 2008, *Nonlinear Continuum Mechanics for Finite Element Analysis*, Cambridge Univ. Press (2008).

[8] Doig, R., Okazawa, S. and Fujikubo, M., 2006, "Solid-fluid interaction analysis by using amulti-material Eulerian finite element method", *Journal of Applied Mechanics JSCE*, Vol. 9, pp. 151–159.